A MODEL AND METHODS FOR REGIONAL TRAVEL-TIME CALCULATION

Stephen C. Myers[1], Sanford Ballard[2], Charlotte A. Rowe[3], Gregory S. Wagner[4], Michael S. Antolik[5], W. Scott Phillips[2], Abe L. Ramirez[1], Mike L. Begnaud[2], Mike E. Pasyanos[1], Doug A. Dodge[1], Megan P. Flanagan[1], Kevin D. Hutchenson[5], Glenn T. Barker[2], John J. Dwyer[4], and David R. Russell[4]

Lawrence Livermore National Laboratory[1], Sandia National Laboratories[2], Los Alamos National Laboratory[3], Air Force Technical Applications Center[4], and Quantum Technology Sciences, Inc.[5]

Sponsored by National Nuclear Security Administration

Contract No. DE-AC52-07NA27344[1], DE-AC04-94AL8500[2], DE-AC52-06NA25396[3], and FA8620-05-C-4301[5]

ABSTRACT

This project develops a model and methods for routine computation of regional travel times for crustal events anywhere on the globe. To improve on existing methods, the travel time calculations must capture the effect of the three-dimensional (3D) earth, yet the computation must be exceedingly efficient. We achieve global coverage by defining a seamless global tessellation of nodes with spacing of approximately 1°. Three-dimensional crustal structure is captured by interpolating P- and S-velocity depth profiles at each node. Mantle structure is approximated by a linear velocity gradient (as a function of depth) at each node. The linear gradient parameterization in the mantle enables an analytical approximation for the diving Pn/Sn ray that allows computation of travel times in approximately 1 millisecond. Regional Pg and Lg propagation are approximated with a ray traveling horizontally along a mid-crustal layer. At local distance, P and S travel times are computed using the layered velocity structure under the station.

The starting model is a hybrid of the Lawrence Livermore National Laboratory (LLNL)/Los Alamos National Laboratory (LANL) unified model, which is a 3D geophysical compilation spanning Eurasia and North Africa, and CRUST2.0 elsewhere. These 3D models are adapted to the linear gradient parameterization using mantle velocities at the Moho and at 130-km depth. At 130-km depth the velocity of is predominantly derived from 2SMAC. We refine the Eurasian and North African portion of the model using a tomographic formulation that adjusts the average crustal velocity, Pn and Sn velocity, and the mantle gradient at each node. Our tomographic data consists of approximately 700,000 validated regional arrivals from events with known locations or locations meeting accuracy criteria. Pn tomography in the Eurasia/North Africa region reduces travel time residual variance by 78%, and additional (noncircular) tests confirm significant improvement in Pn travel time prediction accuracy. Improvement in epicenter accuracy is strongly dependent on network coverage, but improvement of 20%–30% is achieved for networks with azimuthal gap greater than 200°.

Report Documentation Page

Form Approved
OMB No. 0704-0188

1. REPORT DATE	2. REPORT TYPE	3. DATES COVERED
SEP 2008		**00-00-2008 to 00-00-2008**

4. TITLE AND SUBTITLE	5a. CONTRACT NUMBER
A Model and Methods for Regional Travel-Time Calculation	5b. GRANT NUMBER
	5c. PROGRAM ELEMENT NUMBER
6. AUTHOR(S)	5d. PROJECT NUMBER
	5e. TASK NUMBER
	5f. WORK UNIT NUMBER
7. PERFORMING ORGANIZATION NAME(S) AND ADDRESS(ES) **Lawrence Livermore National Laboratory,PO Box 808,Livermore,CA,94551-0808**	8. PERFORMING ORGANIZATION REPORT NUMBER
9. SPONSORING/MONITORING AGENCY NAME(S) AND ADDRESS(ES)	10. SPONSOR/MONITOR'S ACRONYM(S)
	11. SPONSOR/MONITOR'S REPORT NUMBER(S)

12. DISTRIBUTION/AVAILABILITY STATEMENT
Approved for public release; distribution unlimited

13. SUPPLEMENTARY NOTES
Proceedings of the 30th Monitoring Research Review: Ground-Based Nuclear Explosion Monitoring Technologies, 23-25 Sep 2008, Portsmouth, VA sponsored by the National Nuclear Security Administration (NNSA) and the Air Force Research Laboratory (AFRL)

14. ABSTRACT
see report

15. SUBJECT TERMS

16. SECURITY CLASSIFICATION OF:			17. LIMITATION OF ABSTRACT	18. NUMBER OF PAGES	19a. NAME OF RESPONSIBLE PERSON
a. REPORT **unclassified**	b. ABSTRACT **unclassified**	c. THIS PAGE **unclassified**	**Same as Report (SAR)**	**10**	

OBJECTIVES

This project produces a laterally variable velocity model of the crust and upper mantle that is specifically designed for use in routine seismic location. At this time the Seismic Location Baseline Model (SLBM) is focused on travel time prediction at local and regional distances. Therefore, ray paths are wholly within the crust and upper mantle. Like any travel-time prediction method used in a location algorithm, the SLMB must return the following:

1. An accurate travel-time prediction
2. An uncertainty estimate of the travel-time prediction error

Because the SLBM is meant for use in routine location algorithms where networks can be dynamic and precomputation of travel times for all available data may not be possible, the SLBM must also do the following:

3. Compute the travel time on-the-fly, given regional- or local-distance station/event coordinates
4. Return the travel time in milliseconds, thus enabling the estimation of a location in a few seconds

Further, we aim to improve a starting model that is based on a geophysical compilation. The improvement is achieved using a ground-truth dataset and a tomographic technique that is tailored to optimize model parameters important to seismic location.

RESEARCH ACCOMPLISHED

We meet the objectives outlined above by constructing one earth model that is used in the computation of all four regional phases. Further, we adapt several approaches for regional travel time calculation into one software package that provide a convenient travel time calculation utility for use in seismic location and other applications that require a fast and accurate calculation for crustal seismic events. In this paper, we report on methods for computing regional travel times for Pn, Pg, Sn, and Lg phases. We also report on Pn tomography results. Tomography for Pg, Sn, and Lg is in progress.

Model Parameterization

We combine the laterally variable layer approach of Pasyanos et al. (2004) with the linear mantle gradient of Zhao and Xie (1993). Myers et al. (2007) provide model parameterization details, and we summarize here. Velocity vs. depth profiles are defined at nodes, and the profiles at the nodes are interpolated using an efficient code developed at Sandia National Laboratories (SNL) to determine velocity at any arbitrary location (lat,lon,depth). SNL has also developed a tessellation node structure on a spheroid with node spacing of approximately 1° (Figure 1). At present, the model development domain is Eurasia and North Africa, and nodes inside that domain capture the effects of 3D structure on travel times. Outside of the development domain nodes are set to a default velocity profile based on iasp91 (Kennett and Engdahl, 1991). We also have a version of the model that is CRUST2.0 with iasp91 in the mantle and core for the region outside of Eurasia and North Africa. This parameterization provides a seamless and extensible model. Expansion beyond Eurasia and North Africa does not require a change in the model parameterization itself, only modification of the velocity structure at previously defined nodes. Further, SNL has incorporated the GRS80 ellipsoid into the model, eliminating the need for the conventional ellipticity correction to travel time predictions.

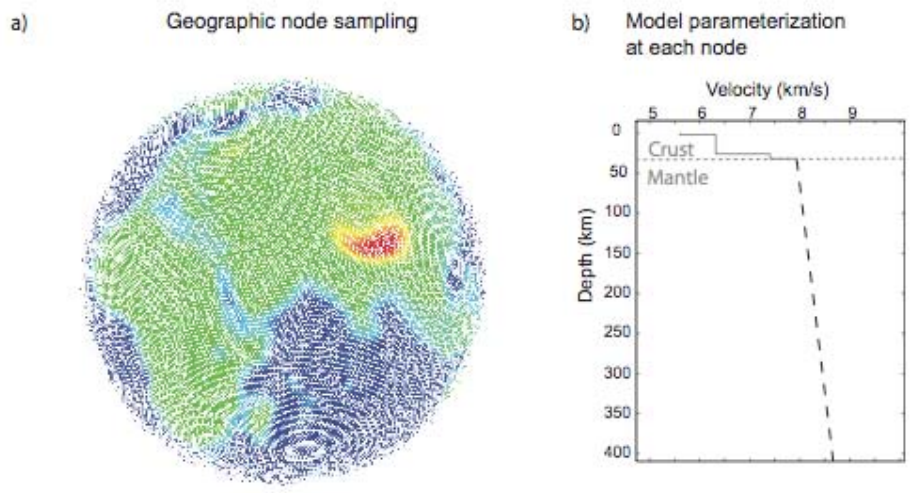

Figure 1. Seismic Location Baseline Model (SLBM) global parameterization. (a) An example tessellation, with approximately 1° grid spacing. Color is based on approximate Moho depth. (b) An example velocity/depth profile as defined at each node. The mantle portion of the profile is specified by the velocity at the crust/mantle interface and a linear gradient.

Travel-Time Calculation, Pn and Sn

The travel-time calculation is based on the method described in Zhao (1993) and Zhao and Xie (1993). This calculation is similar to the widely used approach of Hearn (1984), with an additional term (γ) introduced to account for diving rays that may occur due to a positive velocity gradient with depth and Earth sphericity. The travel time calculation is

$$TT = \sum_{i=1}^{N} d_i s_i + \alpha + \beta + \gamma, \qquad (1)$$

where *d* and *s* are the distance and slowness (taken as 1/mantle MohoVelocity) in each of the *i* segments comprising the great-circle path between Moho pierce points near the event and station, α and β are the crustal travel times at the source and receiver, and γ is a term that accounts for the effect of both mantle velocity gradient and earth sphericity. Figure 2 shows the components of the ray path in a cross section.

We define α as

$$\alpha = \sum_{j=1}^{M} \left[\sqrt{r_j^2 / v_j^2 - p^2} - \sqrt{r_{j+1}^2 / v_j^2 - p^2} \right], \qquad (2)$$

where *v* and *r* are the velocity and layer radius of the *M* crustal layers from the event to the Moho, and *p* is the ray parameter ($p = 1/v$, *v* evaluated at the ray bottoming depth).

We similarly define β as

$$\beta = \sum_{k=1}^{N} \left[\sqrt{r_k^2 / v_k^2 - p^2} - \sqrt{r_{k+1}^2 / v_k^2 - p^2} \right], \qquad (3)$$

where *v* and *r* are defined as above for the *L* crustal layers from the station to the Moho. The same *p* is used in both Eqs. (2) and (3). Because the ray bottoming depth is a function of the pierce point, *p* is determined through an efficient, iterative process.

Per Zhao and Xie (1993),

$$\gamma = -\frac{c^2 Xm^3}{24 V_0} \quad , \tag{4}$$

where X_m is the horizontal distance traveled in the mantle, c is a velocity gradient in the mantle that is normalized by the velocity at the crust mantle boundary plus an additional term to account for Earth sphericity (Helmberger, 1973), and V_0 is a regional average of Pn velocity over the entire study area.

We introduce spatially varying *c* into the model (Phillips et al., 2007), and we calculate γ by averaging c along each ray. V_0 remains an average Pn velocity over the whole model, which allows us to take advantage of linear tomographic inversion methods (see below). Tests suggest that the approximation to V_0 introduces negligible travel time error given Pn velocities ranging from 7.5 km/s to 8.3 km/s.

The Zhao (1993) method is applicable to events in the crust, making the approach well suited to nuclear explosion monitoring. However, seismic location algorithms may explore the possibility that an event occurred in the mantle, necessitating a consistent method of travel time predictions for mantle events. The following extends the travel time method to events in the shallow mantle, with the condition that $c^2h^2 << 1$ (h is the bottoming depth of the ray):

$$TT = \alpha + t_m \tag{5}$$

where α is the crustal travel time from the Moho to the station—as defined in Eq. (2)—and t_m is the travel time in the mantle.

$$t_m = \frac{\left[t_{Moho} \frac{x_m}{d} - \left(\frac{c^2 x_m^2}{24 V_0} \right) \right] \pm \left[t_{Moho} \left(\frac{x_z}{d(1 + c_m z_m)} \right) - \left(\frac{c^2 x_z^2}{24 V_{0z}} \right) \right]}{2} \tag{6}$$

If the ray leaves the event upwards, then the second term in Eq. (6) is subtracted. If the ray leaves the event downwards, then the second term is added. The travel time is t_{Moho} for a ray traversing the Moho from the event to the point where the ray enters the crust and propagates to the station. The horizontal distance is x_m as measured at Moho radius by a ray that starts at the Moho then travels downward passing through the event and continuing to the station. The term x_z is similar to x_m, but the horizontal distance for x_z is measured at the radius of the event. The horizontal distance traveled in the mantle from the event to the Moho pierce point below the station is *d*, as measured at Moho radius. The mantle velocity gradient normalized by average Moho velocity is c_m, with the addition of a term to account for earth sphericity (Helmberger, 1973). The depth of the event below the Moho is z_m. The average model velocity at the depth of the event is V_{0z}.

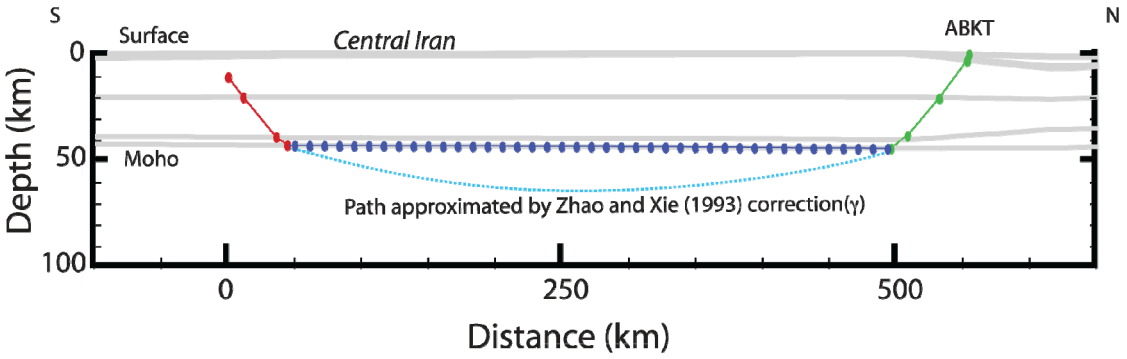

Figure 2. Cross section extracted from the laterally variable SLBM model. The components of the Pn/Sn travel time calculation are also shown. The blue, red, green, and cyan colors correspond to the first, second, third, and fourth terms of Eq. (1).

Travel-Time Calculation, Pg and Lg

Both Pg and Lg phases are trapped in the crust, and both phases exhibit complex waveforms that require hundreds or thousands of rays to model. Further, the first arriving ray with sufficient energy to be observed is dependent on geologic structure and event-station distance. Therefore, it is difficult to physically model the observed travel time using conventional ray techniques. Empirically, Pg and Lg travel at horizontal velocities of approximately 6.0 km/s and 3.2 km/s, respectively, which is suggestive of propagation in the middle crust. Further, event depth can impart a static travel time delay, suggesting a component of propagation from the event to the middle crust then up to the station (for a shallow event). We capture this travel time behavior with a simple approximation, whereby

$$TT = \sum_{i=1}^{N} d_i s_i + \alpha + \beta, \qquad (7)$$

where d_i is the distance traveled in the middle crust in each of N ray segments, α and β propagate the phase to and from the middle crust, respectively. When the source is above the middle crust, then the calculation is almost the same as the Pn/Sn calculation Eq. (1), but the correction for a diving ray is not used. When the source is below the mid-crustal layer, we assume that the ray travels horizontally until Earth sphericity causes the ray to intersect the mid-crustal layer. While this approach by no means captures the physical complexity of Pg and Lg wave propagation, we find that it is suitable for estimating travel time.

The approach described above is suitable for regional travel time calculations. To compute travel times at local distances we approximate the velocity structure with a 1D model (velocity vs. depth) taken at the station of interest. We then use the τ-p approach of Buland and Chapman (1983) to compute travel times in the 1D structure. Using distinct approaches to compute local and regional Pg/Lg travel times necessitates a seamless hand off from one method to the other at the local/regional boundary. For events above the middle crust, we use τ-p if the ray bottoms above the middle crust (Figure 3, left). Mismatch between the local and regional calculations can occur due to differences in the velocity or depth of the middle crust for the local realization (1D) and regional (2D) models. At major tectonic transitions, such as ocean/continent boundaries, the mid-crustal depth and velocity do change rapidly with position, causing the only instances where a mismatch between local and regional travel-time calculations exceeding 0.1 second have been observed.

For events below the middle crust, we compute both the τ-p travel time and the travel time for a ray with slowness determined by the mid-crustal layer. The τ-p calculation is chosen if the ray (1) leaves upward

from the event, *and* (2) the local travel time is greater than the regional calculation. If either condition is not met, then the regional (mid-crustal refraction) calculation is used. These rules for choosing the local or regional calculation produce a piecewise continuous travel-time curve (Figure 3, right). Choosing the longer travel time ensures that the regional ray is (or is close to) geometrical. Figure 3 shows that both the effect of event depth (both locally and regionally) is captured and the effect of laterally varying structure is also captured (e.g., the bends in the regional travel-time curve for the left-hand side of Figure 3).

Tests of travel-time computation time are discussed in Myers et al. (2007). For both Pn/Sn and Pg/Lg computation time is approximately 1 millisecond.

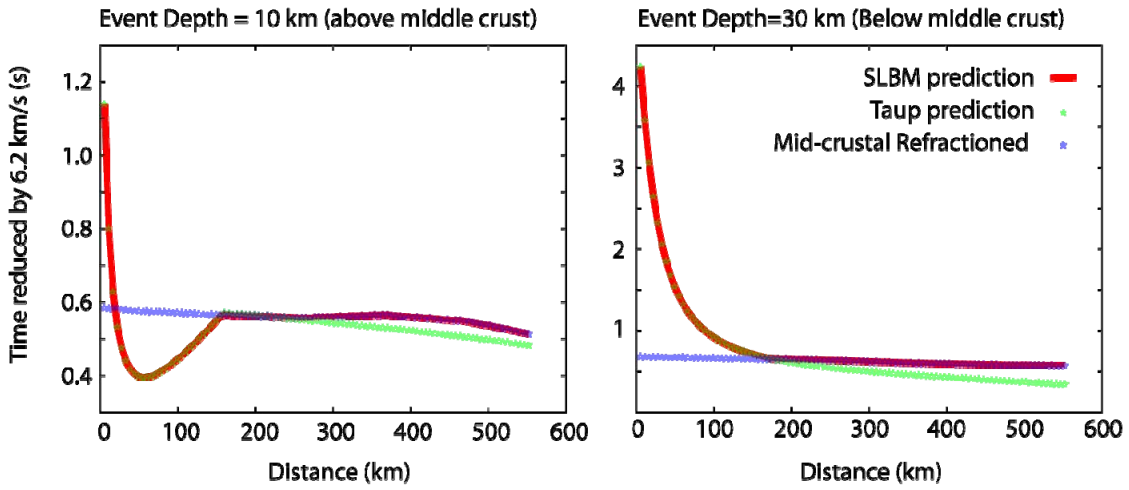

Figure 3. SLBM Pg travel time as a function of distance (red) for an event above the mid-crustal layer (left) and below the mid-crustal layer (right). In both cases the τ-p travel time is shown in green and the mid-crustal refraction is shown in blue. Rules for choosing the local (τ-p) and regional (refraction) travel-time calculation (see text) minimize the discontinuity of the SLBM calculation.

Dataset

The dataset is, arguably, the most-important component of a tomographic study. The dataset must provide the ray-path coverage to constrain the model, and a dataset with small errors in event location and arrival-time measurements helps to improve model resolution. LLNL and LANL have combined ground-truth datasets for this study. Both national laboratories contribute global, regional, and local bulletins (some not widely available), as well as tens of thousands of arrival-time measurements made at the national laboratories. All event locations are evaluated against Bondar et al. (2004) epicenter accuracy criteria, and all picks are evaluated against an error budget that accounts for event mislocation, iasp91 prediction error, and arrival-time measurement error. Observations outside of the 99% confidence bounds for total error are removed. Figure 4 shows the node hit count for Pn rays throughout Eurasia, as well as the resulting tomographic "checkerboard" test for mantle-Moho velocity. The hit count is high (~10,000) throughout the Tethys collision belt (a roughly east-west band from the Pyrenees through the Himalayas). Node hit count to the north of the Tethys collision is also good, with regional bulletins and Soviet peaceful nuclear explosions (PNEs) providing data coverage. Node hit count is poorer south of the Tethys collision, and the starting model will not change significantly. While hit-count is a direct measure of data redundancy, Figure 4b shows that hit-count is also indicative of tomographic resolution.

Tomography

The Pn travel time-formula, Eq. (1) lends itself to tomography. The simple algebra results in a linear tomographic equation.

$$\begin{bmatrix} x_1^1 & \cdots & x_N^1 & -\frac{x_1^1 (X_m)^3}{24 V_O X_m} & \cdots & -\frac{x_N^1 (X_m)^3}{24 V_O X_m} & \sum_{p=1}^{Q} \frac{l_{1p}^1}{v_{1p}} & \cdots & \sum_{p=1}^{Q} \frac{l_{Np}^1}{v_{Np}} \\ \vdots & & & & \ddots & & & \vdots & \\ x_1^K & \cdots & x_N^K & -\frac{x_1^K (X_m)^3}{24 V_O X_m} & \cdots & -\frac{x_N^K (X_m)^3}{24 V_O X_m} & \sum_{p=1}^{Q} \frac{l_{1p}^K}{v_{1p}} & \cdots & \sum_{p=1}^{Q} \frac{l_{Np}^K}{v_{Np}} \\ & & & & \text{Re}\,gularization & & & & \end{bmatrix} * \begin{bmatrix} s_1 \\ \vdots \\ s_N \\ c_1^2 \\ \vdots \\ c_N^2 \\ a_1 \\ \vdots \\ a_N \end{bmatrix} = \begin{bmatrix} T^1 \\ \vdots \\ T^K \\ \text{Re}\,gularization \end{bmatrix}, \qquad (8)$$

where

T	= travel time
s	= Pn slowness
x	= Pn distance (or weight) for each model node
c	= normalized velocity gradient *v = vo(1+cz)*
Xm	= length of Pn path
Vo	= average Pn velocity
v	= velocity of a crustal layer
k	= index on K paths (travel-time observations)
i	= index on N model nodes (mantle path)
j	= index on N model nodes (crustal path)
p	= index on Q crustal layers
a	= scalar adjustment to the crustal slowness stack at each node

This system of equations results in a stable inversion that does not require excessive iteration to convergence. The tomography equation solves for Pn slowness (*s*), mantle velocity gradient (*c*), and a scalar adjustment to crustal slowness (*a*). Solving for laterally variable mantle gradient is similar to the approach presented in Phillips et al. (2007). A significant difference between the formulation presented here and more-typical Pn-tomography formulations is the introduction of a scalar adjustment to the slowness of the crustal stack, as opposed to a static time term to account for errors in crustal travel time. Our goal is to produce a model that improves prediction of travel time along the whole ray path, and adjusting crustal slowness better meets our goal.

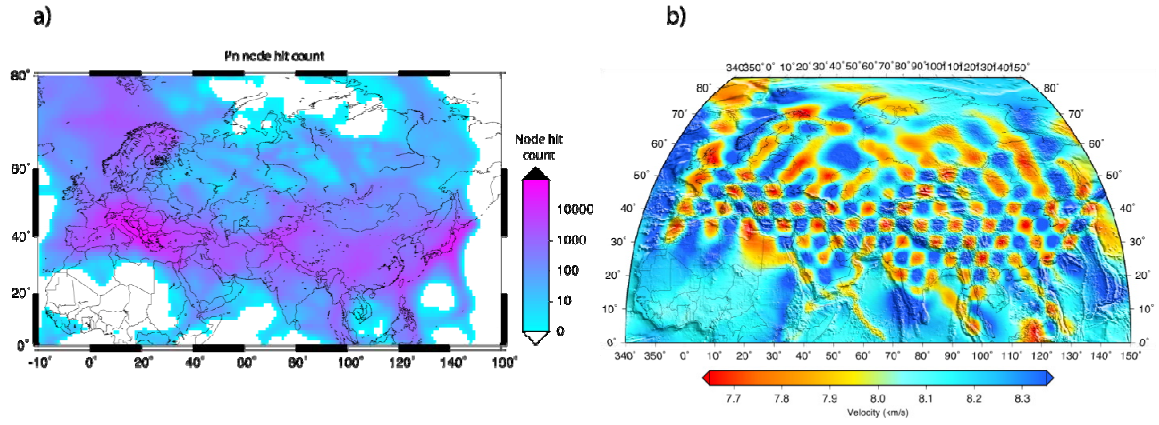

Figure 4. (a) Node hit count for Pn rays. (b) Tomographic checkerboard test for the Pn dataset.

Pn tomography results are presented in Figure 5. Across much of Eurasia and North Africa, starting model anomalies are enhanced and anomaly boundaries are altered by tomography. In the Scandinavian and Siberian shields, Pn velocity is higher than the starting model. Tomographic velocity is slower than the starting model across much of East Asia, and velocities are significantly reduced from the starting model in the Pacific subduction zones. Figure 5c shows that crustal velocities are not significantly changed from the starting model. The starting model features variable crustal thickness and laterally varying velocity. Further, smoothness constraints inhibit lateral variation of the crustal correction. Figure 5d shows that the P-wave velocity gradient varies considerably. The strongest gradients are seen in convergent zones, such as the Pacific subduction zones, Himalayan collision, and the Zagros Mountains and the Mediterranean subduction zones. Gradients are low in backarcs and moderate across large portions of the continental interior.

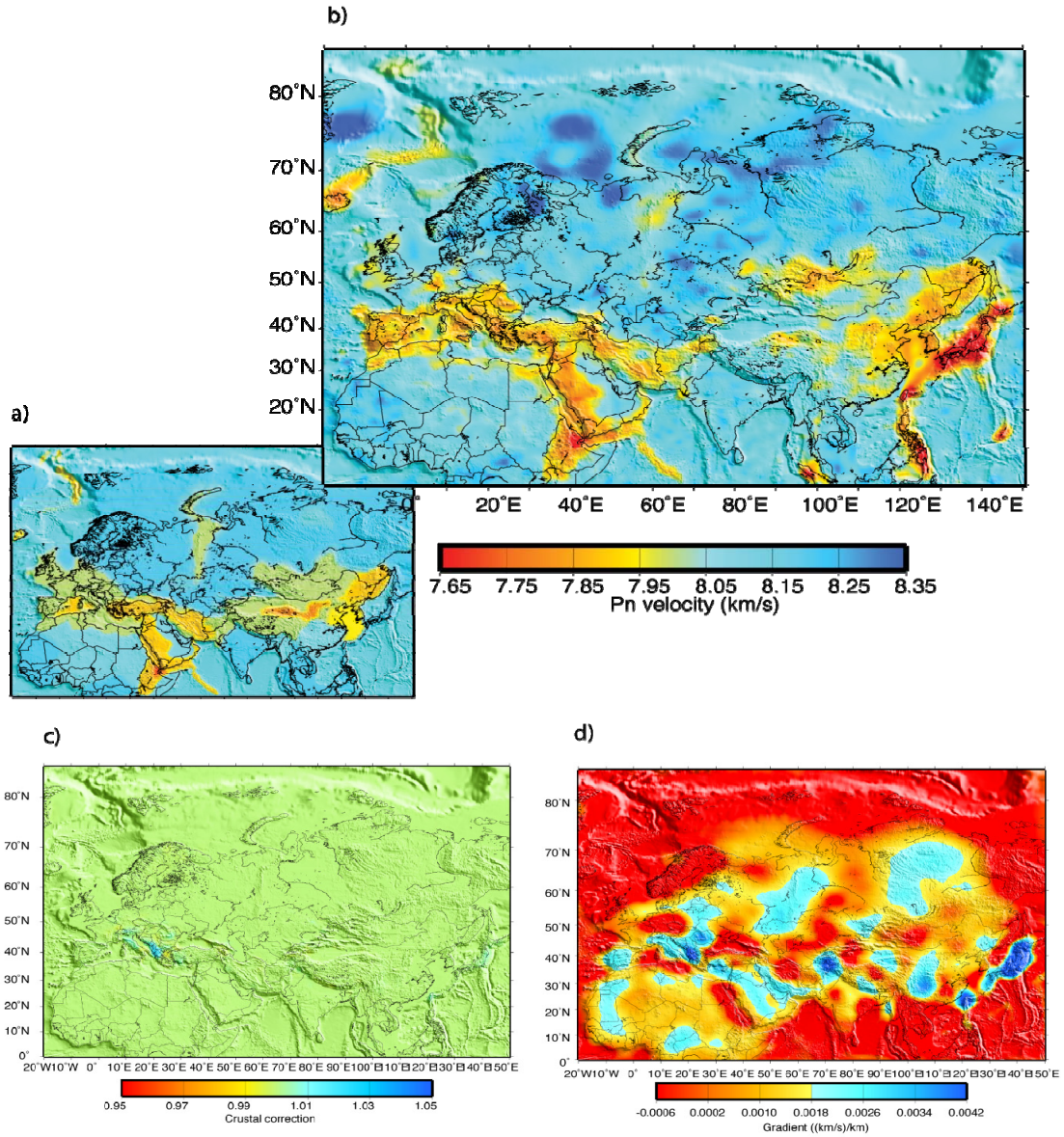

Figure 5. Tomographic results. (a) Pn starting model. (b) Pn tomography model. (c) Pn tomography crustal correction (*a* in Eq. [8]). (d) Tomographic P-wave velocity gradient. See text for discussion.

Figure 6 shows improvement of travel time prediction and epicenter estimation using the SLBM tomography. Figure 6a shows that *iasp91* model error (from Flanagan et al., 2007) is significantly higher at regional distance than at teleseismic distance (>~20°). SLBM tomography reduces Pn travel time prediction to approximately 1.25 seconds, making region travel time prediction error similar to teleseismic prediction error. Figure 6b reaffirms that model error does not significantly affect epicenter error when stations surround the event (Bondar et al., 2004). When network azimuthal gap increases, as is likely for a sparse regional network, SLBM tomography measurably improves epicenter accuracy. For azimuthal gap greater than 200°, SLBM improves epicenter accuracy by approximately 30%.

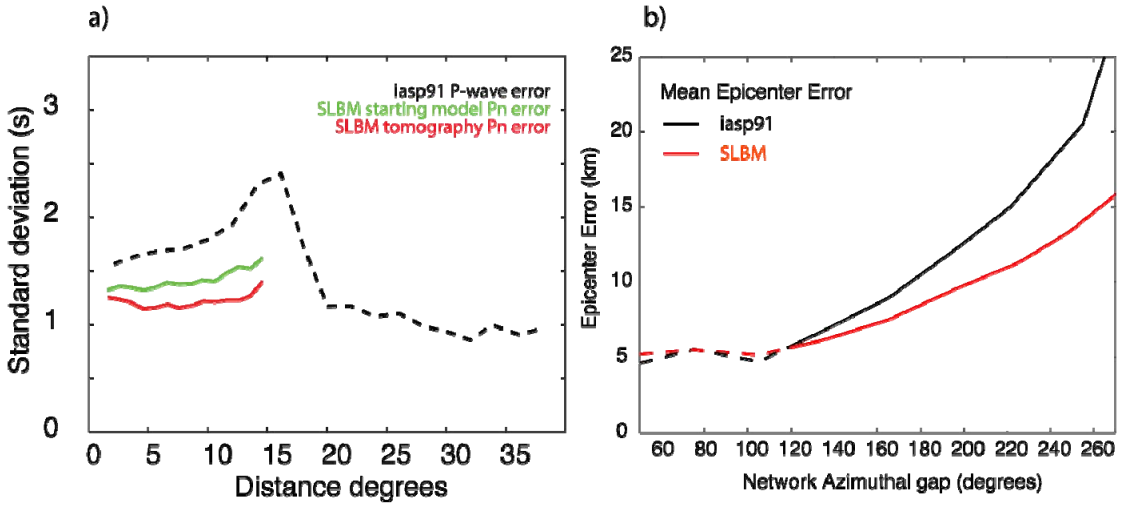

Figure 6. Pn tomography validation results. (a) Travel-time error vs. event-station distance for the iasp91 (black), the SLBM starting model (green), and the SLBM tomography (red). (b) Mean epicenter error as a function of network azimuthal gap for iasp91 (black) and the SLBM tomography (red). See text for discussion.

CONCLUSIONS AND RECOMMENDATIONS

We describe the progress of the SLBM project to date. This project is distinct because it tailors the travel-time prediction algorithm and tomography results for use in routine seismic location algorithms. Emphasis is placed on travel-time prediction accuracy and computational efficiency of regional phases.

The tessellation model parameterization provides seamless global coverage. The use of a tessellation approach also allows fast interpolation of model parameters to extract the great-circle cross section of velocity structure that is needed to compute regional travel times. The current focus of the SLBM effort is Eurasia and North Africa, and model nodes outside of that area are set to a default velocity structure consisting of CRUST 2.0 (Bassin et al., 2000) with iasp91 for the mantle (Kennett and Engdahl, 1991). We note that the model is extensible, and a global calibration effort would entail updating node-centered velocity profiles (by whatever means), which does not require updates to the model tessellation or travel-time codes.

We make use of several approximations that result in a relatively simple algebraic form for travel-time calculations, Eq. (1). The algebraic form lends itself to a linear tomographic formulation, Eq. (8). LLNL and LANL have merged ground-truth databases to form a tomography dataset for this project. Pn ray coverage across Eurasia and North Africa is excellent (Figure 4). Pn tomographic results (Figure 5) are in general agreement with studies of the Eurasian subregions.

Tests of Pn tomography travel-time prediction show that Pn model error is reduced to approximately 1.25 seconds, and the error is relatively constant (stationary) with distance. Reducing regional travel-time prediction error to approximately the level of teleseismic error (~1 second) allows the joint use of regional and teleseismic data in event location without degrading epicenter accuracy. Epicenter accuracy improves by approximately 30% (relative to iasp91) for large network azimuthal gaps (i.e., when the stations are to one side of the event).

Tomographic efforts for Pg, Sn, and Lg are underway.

ACKNOWLEDGEMENTS

This project would not be possible without the full support of Leslie Casey in the Department of Energy office of NA22. Steve Myers also wishes to thank Dave Harris for daily interactions and general technical discussions.

REFERENCES

Bassin, C., G. Laske, and G. Masters (2000). The current limits of resolution for surface wave tomography in North America, *EOS Tran.s AGU* 81: F897.

Bondar, I., S. Myers, E. R. Engdahl, and E. Bergman, (2004). Epicenter accuracy based on seismic network criteria, *Geophys. J. Int.* 156: 483–496.

Buland, R. and C. H. Chapman (1983). The computation of seismic travel times, *Bull. Seismol. Soc. Am.*, 73: 1271–1302.

Flanagan, M.P., S.C. Myers, and K.D. Koper (2007). Regional travel-time uncertainty and seismic location improvement using a three-dimensional a priori velocity model, *Bull. Seismolog. Soc. Am*. 97: 804–825.

Hearn, T. M. (1984). Pn travel times in southern California, *Jour. Geophys. Res*. 89: 1843–1855.

Helmberger, D. V. (1973). Numerical seismograms of long-period body waves from seventeen to forty degrees, *Bull. Seism. Soc. Am*. 63: 633–646.

Kennett, B. L. N. and E. R. Engdahl, (1991). Traveltimes for global earthquake reference location and phase identification, *Geophys. J. Int.* 105: 429–465.

Myers, S. C., S. Ballard, C. Rowe, G. Wagner, M. Antolik, S. Phillips, A. Ramirez, M. Begnaud, M. Pasyanos, D. Dodge, M. Flanagan, K. Hutchenson, G. Barker, J. Dwyer, and D. Russell (2007). Tomography and methods of travel-time calculation for regional seismic location, in *Proceedings of the 29th Seismic Research Review: Ground-Based Nuclear Explosion Monitoring Technologies*, LA-UR-07-5613, Vol. 1, pp. 414–423.

Pasyanos, M. E., W. R. Walter, M. P. Flanagan, P. Goldstein, and J. Bhattacharyya (2004). Building and testing an a priori geophysical model for western Eurasia and North Africa, *Pure App. Geophys*. 161: 235–281.

Phillips, W. S., M. L. Begaud, C. A. Rowe, L. K. Steck, S. C. Myers, M. E. Pasyanos, and S. Ballard (2007). Accounting for lateral variations of the upper mantle gradient in Pn tomography studies, *Geophys. Res. Lett*. 34: doi:10.1029/2007GL029338.

Zhao, L.-S. (1993). Lateral variations and azimuthal isotropy of Pn velocities beneath Basin and Range province, *J. Geophys. Res*. 98:109–122.

Zhao and Xie (1993). Lateral variations in compressional velocities beneath the Tibetan Plateau from Pn traveltime tomography, *Geophys. J. Int*. 115: 1070–1084.